ModMax charged black holes in PFDM: Electric Penrose and particle collisions

Nuriddin Kurbonov[1,2,3†] Mukhabbat Kurbanova[4,5‡] Javlon Rayimbaev[6,7§] Yunus Turaev[8♮]
Sulton Usanov[9♯] Saidmuhammad Ahmedov[10¶]

[1]Institute for Advanced Studies, New Uzbekistan University, Movarounnahr str. 1, Tashkent 100000, Uzbekistan
[2]University of Tashkent for Applied Sciences, Str. Gavhar 1, Tashkent 100149, Uzbekistan
[3]Tashkent State Technical University, Tashkent 100095, Uzbekistan
[4]Institute of Fundamental and Applied Research, National Research University TIIAME, Kori Niyoziy 39, Tashkent 100000, Uzbekistan
[5]American University of Technology, Beshyogoch street 1, Tashkent 100060, Uzbekistan
[6]Institute of Theoretical Physics, National University of Uzbekistan, Tashkent 100174, Uzbekistan
[7]Samarkand State University, University blv.15, Samarkand 140104, Uzbekistan
[8]Mamun University, Bolkhovuz Street 2, Khiva 220900, Uzbekistan
[9]Kimyo International University in Tashkent, Shota Rustaveli street 156, Tashkent 100121, Uzbekistan
[10]National University of Uzbekistan, Tashkent 100174, Uzbekistan

Abstract: In this study, we investigate the influence of the parameters of ModMax nonlinear electrodynamics and perfect-fluid dark matter (PFDM) on the geometry and physical properties of charged black holes. A static, spherically symmetric solution to the Einstein field equations describing a charged ModMax black hole immersed in a PFDM background is obtained. The motion of charged test particles in this spacetime is analyzed in detail, including the effective potential, the conditions for stable and unstable circular orbits, and the radius of the innermost stable circular orbit (ISCO). It is shown that the ModMax parameter γ shifts the orbits outward for repulsive Coulomb interactions and inward for attractive forces, while increasing PFDM enhances gravitational attraction, shifting the ISCO inward. Furthermore, the interactions and collisions of charged particles near the event horizon are examined. The center-of-mass energy $\mathcal{E}_{cm}$ exhibits the characteristic behavior in charged-particle collisions, rapidly increasing as the particles approach the horizon. The parameter γ amplifies the BSW acceleration mechanism, while α suppresses it. The electric Penrose process for charged particles is also examined, revealing that the efficiency of energy extraction increases with the black hole charge and is strongly influenced by the interaction parameter γ, which plays a dominant role in enhancing the efficiency, whereas the effect of α remains comparatively negligible.

Keywords: ModMax electrodynamics, charged black holes, Electric Penrose & particle collisions, PFDM

DOI: 10.1088/1674-1137/ae5b56 **CSTR:**

CPC Accepted

I. INTRODUCTION

The study of black holes and their interaction with fundamental fields has become a cornerstone of modern theoretical physics. Among recent developments, the ModMax theory, a nonlinear and duality-invariant conformal extension of Maxwell electrodynamics, provides a fertile framework for investigating black hole spacetimes and gravitational waves sourced by nonlinear electromagnetic fields [1, 2]. Such modifications preserve duality symmetry while allowing richer dynamics, thereby opening new possibilities for understanding strong-field regimes in which conventional Maxwell theory may be insufficient [3, 4]. The implications of these extensions for astrophysical black holes, gravitational-wave emission, and near-horizon physics are actively being explored [5−10].

The ModMax theory represents a novel one-parameter extension that maintains both SO(2) duality invariance [11] and conformal invariance, distinguishing it from oth-

Received 20 November 2025; Accepted 2 April 2026
† E-mail: Electronic address: n.kurbonov@newuu.uz
‡ E-mail: Electronic address: kmukhabbat98@gmail.com
§ E-mail: Electronic address: javlon@astrin.uz
♮ E-mail: Electronic address: yunus.turaev.nw@gmail.com
♯ E-mail: Electronic address: usanovsulton@gmail.com
¶ E-mail: Electronic address: saidmuhammadaxmed@gmail.com
©2026 Chinese Physical Society and the Institute of High Energy Physics of the Chinese Academy of Sciences and the Institute of Modern Physics of the Chinese Academy of Sciences and IOP Publishing Ltd. All rights, including for text and data mining, AI training, and similar technologies, are reserved.

er nonlinear electrodynamics (NED) such as Born–Infeld or Euler–Heisenberg, which introduce fixed energy scales that break conformality [2]. Parameterized by γ, ModMax reduces to Maxwell electrodynamics when $\gamma = 0$, but for nonzero γ it introduces interactions while admitting exact lightlike plane-wave solutions of arbitrary polarization. In the weak-field limit, small-amplitude waves on constant backgrounds exhibit birefringence, with one mode propagating at light speed and the other subluminal for $\gamma > 0$, which ensures causality; we therefore restrict to positive γ [12−16]. The Hamiltonian and Lagrangian formulations reveal a self-dual structure built from the invariants s and p. The theory's non-analyticity at vacuum configurations underscores its unique properties. When coupled to general relativity, ModMax sources self-gravitating configurations, including charged black holes with Reissner–Nordström-like (RN) metrics, in which the nonlinearity parameter γ effectively screens the charge, allowing extremal black holes with mass smaller than the absolute value of the charge [1, 17, 18]. Related developments include exact self-gravitating ModMax solutions, black-hole configurations in conformal nonlinear electrodynamics, and slowly rotating black-hole extensions, which further illustrate the richness of the theory in gravitational settings [19−21]. Birefringence in these waves manifests through distinct optical metrics for photon modes, providing a framework for studying conformal NEDs [22] in gravitational contexts. This integration provides insights into high-energy physics, the potential for regular black holes, and cosmological implications, thereby bridging the realms of electromagnetic and gravitational phenomena in extreme regimes.

Another line of research explores the role of dark matter (DM) in shaping the environments of black holes (BHs) and galaxies. The dark matter parameter α influences horizon equations, constraining its range based on the cosmological constant Λ; for positive Λ, horizons include cosmological ones, while negative Λ alters extremality bounds [23, 24]. The ergosphere, essential for energy extraction, shrinks with increasing $|\alpha|$ and is particularly affected by high dark matter densities near the BH, whereas dark energy has minimal impact. Singularities remain ring-like, unaffected by perfect fluid dark matter (PFDM), and geodesic analyses reveal stable equatorial orbits with asymptotically flat rotational velocities for $\alpha > 0$. Models incorporating PFDM backgrounds into Kerr-(anti-)de Sitter solutions reveal nontrivial modifications to the geometry and thermodynamics of rotating BHs [25]. In addition, scalar-field-inspired models, such as quintessential dark matter and phantom field descriptions, have been proposed to account for flat galactic rotation curves and cosmic acceleration without invoking conventional cold dark matter [26−29]. These approaches highlight the significance of matter fields with exotic properties in shaping both local astrophysical processes and large-scale cosmological dynamics.

The Penrose process provides the prototype for extracting rotational energy from a Kerr black hole through particle splitting in the ergosphere, where negative-energy states relative to infinity can occur [30, 31]. Particle-based extensions of this idea include the magnetic, electric, and radiative Penrose processes, in which electromagnetic interactions allow charged particles or emitted photons to participate in the extraction mechanism [31−33]. These variants should be distinguished from the Blandford–Znajek mechanism, which is a field-based process that extracts black-hole rotational energy via electromagnetic stresses in a magnetized plasma [34, 35]. In the generalized Penrose-process viewpoint, the Blandford–Znajek mechanism may be interpreted as a collective electromagnetic counterpart of Penrose-type extraction, governed by negative-energy and negative-angular-momentum flux into the black hole [35]. Because of its efficiency in magnetized accretion flows, the Blandford–Znajek process is widely invoked in discussions of relativistic jets and related high-energy astrophysical phenomena [34, 36−39]. In this work, we are particularly interested in how gravitational, electromagnetic, and dark-sector effects modify the efficiency and observational signatures of such energy-extraction channels.

BHs, characterized by their rotation, serve as natural particle accelerators capable of producing collisions with arbitrarily high center-of-mass energies near their horizons [40]. The study of charged-particle dynamics, characteristic circular orbits, and collision processes in non-standard BH backgrounds has therefore become an important theoretical tool for understanding how modifications to the geometry and matter sectors affect strong-field behavior [41, 42]. While physical constraints such as backreaction, astrophysical limitations, and nonlinear interactions regulate this effect, the framework offers deeper insights into the fundamental limits of energy extraction and the potential interplay with modified electromagnetic and dark matter scenarios. The Bañados-Silk-West (BSW) effect requires one particle to have near-critical angular momentum, balancing gravitational attraction and centrifugal repulsion, while the other falls freely; practical limits arise from backreaction, radiation losses, and non-extremality, capping energies at 10^{20} eV for astrophysical BHs. Taken together, these directions form a coherent picture in which modifications to classical fields, dark matter models, and energy-extraction mechanisms converge to provide new perspectives on BH physics and its astrophysical manifestations.

In this paper, we investigate a static, spherically symmetric, charged BH solution derived from ModMax nonlinear electrodynamics and embedded in a PFDM background.

The paper is organized as follows. Section II presents

CPC Accepted

the charged ModMax BH solution in a PFDM background and reviews its geometric properties. Section III analyzes the dynamics of charged particles in this spacetime, with special emphasis on the innermost stable circular orbit (ISCO). Section IV is devoted to the study of the electric Penrose process. Subsequently, Section V investigates collisions of charged particles in the vicinity of the charged ModMax BH surrounded by PFDM. Finally, we summarize the main results and discuss their physical implications.

We adopt geometrized units with $G_{\rm N}=c=1$ and employ the spacetime signature $(-,+,+,+)$. The parameters of the system are defined as follows: M denotes the ADM mass, Q the electric charge, γ the ModMax deformation parameter, and α the PFDM strength parameter, which may assume either positive or negative values depending on the underlying dark matter model. Unless otherwise specified, Greek indices are taken to range over $0-3$, while Latin indices are restricted to the spatial range $1-3$.

II. CHARGED MODMAX BLACK HOLE SOLUTION IN PFDM

The most compact and straightforward way to present the theory is through the action.

$$\mathcal{S}=\frac{1}{2}\int d^4x\sqrt{-g}\,[R+\mathcal{L}_{\rm ModMax}+\mathcal{L}_{\rm PFDM}], \tag{1}$$

where R denotes the Ricci scalar. The ModMax Lagrangian depends on the electromagnetic invariants.

$$S\equiv-\frac{1}{4}F_{\mu\nu}F^{\mu\nu},\quad P\equiv-\frac{1}{4}F_{\mu\nu}\tilde{F}^{\mu\nu}, \tag{2}$$

and has the form [2]

$$\mathcal{L}_{\rm ModMax}=\cosh\gamma\, S+\sinh\gamma\,\sqrt{S^2+P^2}. \tag{3}$$

A practical way to analyze the ModMax field is to introduce the Plebański dual variable defined by

$$\begin{aligned}\mathcal{P}_{\mu\nu}&=-\mathcal{L}_S F_{\mu\nu}-\mathcal{L}_P\tilde{F}_{\mu\nu}\\&=\left(\cosh\gamma-\frac{S}{(S^2+P^2)^{1/2}}\sinh\gamma\right)F_{\mu\nu}-\frac{P\sinh\gamma}{(S^2+P^2)^{1/2}}\tilde{F}_{\mu\nu}.\end{aligned} \tag{4}$$

The dual of $\mathcal{P}_{\mu\nu}$ is then given by:

$$\tilde{\mathcal{P}}_{\mu\nu}=\left(\cosh\gamma-\frac{S}{(S^2+P^2)^{1/2}}\sinh\gamma\right)\tilde{F}_{\mu\nu}+\frac{P\sinh\gamma}{(S^2+P^2)^{1/2}}F_{\mu\nu}. \tag{5}$$

The ModMax theory is distinguished by its invariance under conformal transformations of the metric, $g\to\Omega^2 g$.

$$\begin{pmatrix}\mathcal{P}'_{\mu\nu}\\ \tilde{F}'_{\mu\nu}\end{pmatrix}=\begin{pmatrix}\cos\theta & \sin\theta\\ -\sin\theta & \cos\theta\end{pmatrix}\begin{pmatrix}\mathcal{P}_{\mu\nu}\\ \tilde{F}_{\mu\nu}\end{pmatrix}, \tag{6}$$

with

$$\mathcal{P}=\left(\cosh\gamma-\frac{S\sinh\gamma}{\sqrt{S^2+P^2}}\right)F-\frac{P\sinh\gamma}{\sqrt{S^2+P^2}}\tilde{F}. \tag{7}$$

ModMax configurations with vanishing electromagnetic invariant S reduce to the corresponding solutions of Maxwell electrodynamics. This correspondence applies, for example, to static, purely electric or purely magnetic configurations. By contrast, when both electric and magnetic charges are present, even static, spherically symmetric solutions can depart nontrivially from their Maxwell analogues, as shown in [1, 19] (see also [20] for Taub–NUT–type solutions). Moreover, upon introducing slow rotation, the intrinsic nonlinearity of ModMax becomes unavoidable [21]; to date, an exact solution for the fully rotating case remains unavailable.

In the purely electrostatic, spherically symmetric case, one has $P=0$ and, choosing the branch consistent with the sign of the electromagnetic field, the combination in Eq. (3) effectively reduces to a rescaling of the Maxwell term, so that the constitutive derivative with respect to S is constant. In particular, for the electrostatic branch, one obtains $\mathcal{L}_S\equiv\partial\mathcal{L}_{\rm ModMax}/\partial S=e^{\gamma}$.

Varying the action with respect to the metric and the vector potential yields the Einstein equations.

$$G_{\mu\nu}=R_{\mu\nu}-\frac{g_{\mu\nu}}{2}R=T^{(\rm ModMax)}_{\mu\nu}+T^{(\rm PFDM)}_{\mu\nu}, \tag{8}$$

$$\partial_\mu\left(\sqrt{-g}\tilde{E}^{\mu\nu}\right)=0, \tag{9}$$

where $T^{\rm ModMax}_{\mu\nu}$ denotes the energy-momentum tensor of the ModMax theory, $T^{\rm PFDM}_{\mu\nu}$ denotes that of PFDM, and $\mathcal{R}_{\mu\nu}$ is the Ricci tensor; in addition, the fields satisfy generalized Maxwell-like equations for nonlinear electrodynamics

$$\nabla_\mu\left(\mathcal{L}_S F^{\mu\nu}+\mathcal{L}_P\tilde{F}^{\mu\nu}\right)=0. \tag{10}$$

In the electrostatic case, $\mathcal{L}_P=0$ and $\mathcal{L}_S=e^{\gamma}$, so that Eq. (10) can be readily integrated in spherical symmetry.

The energy-momentum tensor for the ModMax theory is given by

CPC Accepted

$$4\pi T^{\mu\nu}_{ModMax} = \left(F^{\mu\sigma}F^{\nu}_{\sigma}e^{-\gamma}\right) - e^{-\gamma}S\,g^{\mu\nu} \tag{11}$$

with

$$\tilde{E}_{\mu\nu} = \frac{\partial \mathcal{L}}{\partial F^{\mu\nu}} = 2\left(\mathcal{L}_S F_{\mu\nu}\right) \tag{12}$$

where $\mathcal{L}_S = \dfrac{\partial \mathcal{L}}{\partial S}$.

In the electrically charged case, the Maxwell–like stress–energy tensor in Eq. (11) depends on the factor $e^{-\gamma}$. Consequently, the generalized Maxwell equations reduce to the standard Maxwell equations with an effective electromagnetic coupling rescaled by the parameter γ, and the corresponding stress–energy tensor retains the Maxwell form with the effective charge $e^{-\gamma}Q$, which depends on γ and the charge.

For a purely electric configuration, the conserved-charge equation (9) takes the form:

$$\partial_\mu\left(\sqrt{-g}e^{-\gamma}F^{\mu\nu}\right) = 0. \tag{13}$$

The PFDM contribution is modeled as an effective, static, spherically symmetric, anisotropic fluid, with its exterior imprint encoded in the parameter α. In a spherically symmetric background, the corresponding stress-energy tensor can be written in an orthogonal basis as [26, 27, 43]

$$T^{(\mathrm{PFDM})}_{\mu\nu} = \mathrm{diag}[-\epsilon, P_r, P_\theta, P_\phi], \tag{14}$$

with $P_\theta = P\phi$. For the PFDM metric considered here, substitution into the Einstein equations determines the effective source to be of the form

$$-\epsilon = P_r = \frac{\alpha}{8\pi r^3}, \qquad P_\theta = P_\phi = -\frac{\alpha}{16\pi r^3}. \tag{15}$$

Thus, this energy-momentum tensor is not introduced arbitrarily but represents an effective, anisotropic matter distribution consistent with the static geometry of the PFDM spacetime. For simplicity, we denote the PFDM parameter by α, which characterizes the strength of the dark matter contribution.

We adopt the standard static, spherically symmetric ansatz in Schwarzschild coordinates.

$$ds^2 = -f(r)dt^2 + \frac{dr^2}{f(r)} + r^2\left(d\theta^2 + \sin^2\theta\, d\phi^2\right). \tag{16}$$

The field equations (8), together with the metric function (16), can be concisely represented by the following set of differential equations:

$$G_{tt} = G_{rr} = rf'(r) + f(r) - \frac{\alpha}{r} - \frac{2Q^2e^{-\gamma}}{r^3} - 1 \tag{17}$$

$$G_{\theta\theta} = G_{\phi\phi} = rf''(r) + 2f'(r) + \frac{\alpha}{r^2} + \frac{Q^2e^{-\gamma}}{r^2} \tag{18}$$

where G_{tt}, G_{rr}, $G_{\theta\theta}$, and $G_{\phi\phi}$ are, respectively, the tt, rr, $\theta\theta$, and $\phi\phi$ components of the field equations in Eq. (8), and the solution can be immediately obtained following [25, 26]

$$f(r) = 1 - \frac{2M}{r} + \frac{e^{-\gamma}Q^2}{r^2} + \frac{\alpha}{r}\ln\frac{r}{|\alpha|}, \tag{19}$$

and by the electrostatic potential

$$A_t(r) = -\frac{e^{-\gamma}Q}{r}. \tag{20}$$

The logarithmic term in Eq. (19) uses $|\alpha|$ to guarantee a real-valued argument for all $\alpha \neq 0$, thus accommodating both positive and negative values commonly encountered in PFDM models. Equation (19) interpolates between several well-known limits:

- $\alpha = 0$: a charged ModMax black hole in vacuum with an effective charge squared of $e^{-\gamma}Q^2$;
- $\gamma = 0$: PFDM-deformed RN-like solution.
- $\alpha = \gamma = 0$: the standard RN geometry.

The parameter α encodes the influence of PFDM: the term $\frac{\alpha}{r}\ln\frac{r}{|\alpha|}$ modifies the asymptotic fall-off compared to the pure Schwarzschild/RN cases and produces a mild logarithmic correction at large radii, with $\alpha < 0$ typically enhancing gravitational attraction.

Figure 1 shows the dependence of the event-horizon radius r_h of ModMax charged black holes in PFDM on the electric charge Q. In the top panel, with fixed α, r_h gradually decreases as Q increases; however, the rate of this decrease slows with growing γ. At small γ, r_h drops rapidly, whereas at large γ it falls slowly, reflecting the weakening of the effective charge contribution to the metric ($\sim e^{-\gamma}Q^2/r^2$) due to ModMax nonlinearity. Thus, at the same Q, higher γ increases r_h, allowing the black hole to sustain a larger charge before reaching the extremal limit. In the bottom panel, with fixed γ, r_h also decreases with charge, but the rate of decline accelerates with increasing α. For small α, the drop is slow; for larger α, it is faster due to the enhanced PFDM contribution via the term $\sim \frac{\alpha}{r}\ln\frac{r}{|\alpha|}$, which increases the effective mass

CPC Accepted

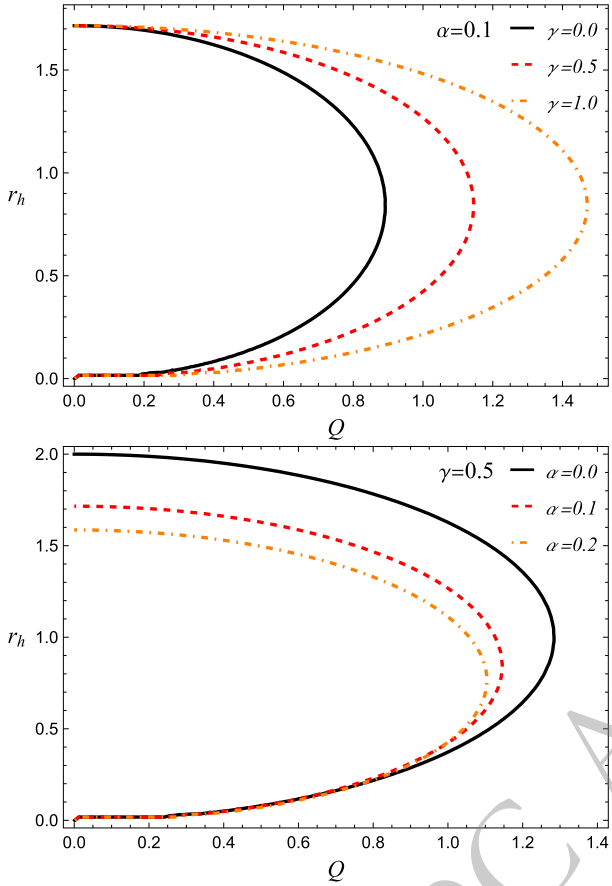

Fig. 1. (color online) Event-horizon radius as a function of the black-hole charge for various values of the ModMax and PFDM parameters. The upper and lower curves correspond to the outer and inner horizons, respectively.

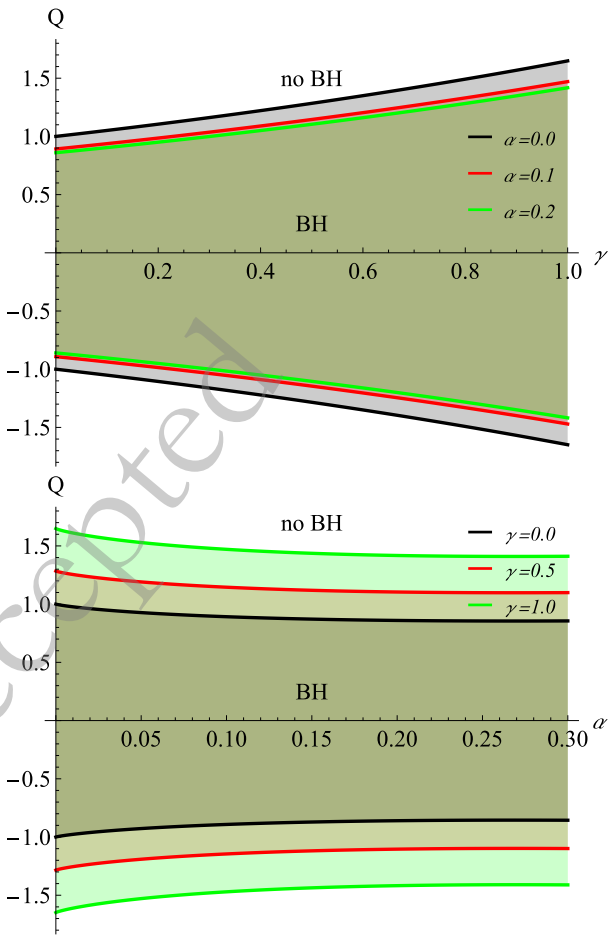

Fig. 2. (color online) Dependence of the extremal electric charge Q of ModMax-charged black holes in PFDM on the parameters α and γ.

CPC Accepted

and compresses the horizon, resulting in a smaller r_h at the same Q and pushing the system toward extremality at lower charges.

Figure 2 illustrates the extremal charge $Q_{\rm ext}$ at which the inner and outer horizons of the charged ModMax BH in PFDM coincide. The boundary at $Q_{\rm ext}$ separates two fundamental regimes: BH solutions exist only for $|Q| < Q_{\rm ext}$ (below the curves), whereas naked singularities arise for $|Q| > Q_{\rm ext}$ (above the curves). This defines a critical charge-to-mass ratio that is modulated by the NED and the surrounding dark-matter environment.

The top panel shows that increasing γ raises $Q_{\rm ext}$, allowing the BH to accumulate larger charge before reaching the extremal limit. This stems from the $e^{-\gamma}$ screening factor in ModMax theory, which exponentially weakens the effective electromagnetic repulsion near the horizon. Consequently, a positive γ is necessary for the existence of superextremal configurations. In contrast, the bottom panel shows that increasing α slightly lowers $Q_{\rm ext}$, reflecting the attractive gravitational pull of the PFDM, which counteracts charge repulsion and favors extremality at smaller $|Q|$. Thus, γ and α have opposite effects on the horizon structure, i.e., increasing γ increases the extremal charge $Q_{\rm ext}$ and thereby enlarges the region of parameter space admitting an event horizon, whereas increasing α slightly decreases $Q_{\rm ext}$ and reduces the range of Q for which a black hole (rather than a naked singularity) solution exists.

III. CHARGED PARTICLES DYNAMICS

We now derive the first integrals of motion for a point particle of mass m and charge q in the background described by Eq. (16) with electromagnetic potential given by Eq. (20). The worldline Lagrangian is

$$\mathcal{L} = \frac{1}{2} m g_{\mu\nu} \dot{x}^\mu \dot{x}^\nu + q A_\mu \dot{x}^\mu, \tag{21}$$

where an overdot denotes differentiation with respect to the proper time τ.

The canonical momenta are

$$p_t = mg_{tt}\dot{t} + qA_t = -E, \tag{22}$$

$$p_\phi = mg_{\phi\phi}\dot{\phi} = L. \tag{23}$$

Hence, the conservation of energy and angular momentum yields the following:

$$\dot{t} = \mathcal{E} + \frac{qA_t(r)}{mf(r)}, \tag{24}$$

$$\dot{\phi} = \frac{\mathcal{L}}{r^2\sin^2\theta}. \tag{25}$$

where $\mathcal{L} = L/m$ and $\mathcal{E} = E/m$.

The normalization condition is:

$$g_{\mu\nu}\dot{x}^\mu\dot{x}^\nu = -\sigma, \quad \sigma = \begin{cases} 1, & \text{timelike} \\ 0, & \text{null} \end{cases} \tag{26}$$

By substituting Eqs. (24)–(25) into Eq. (26), we obtain the radial equation.

$$\dot{r}^2 = \left(\mathcal{E} + \frac{qA_t(r)}{m}\right)^2 - f(r)\left(\sigma + r^2\dot{\theta}^2 + \frac{\mathcal{L}^2}{r^2\sin^2\theta}\right). \tag{27}$$

Owing to spherical symmetry, we can restrict the motion to the equatorial plane $\theta = \pi/2$, with $\dot{\theta} = 0$. Then

$$\dot{t} = \frac{\mathcal{E}}{f(r)} - \frac{qe^{-\gamma}Q}{mrf(r)}, \quad \dot{\phi} = \frac{\mathcal{L}}{r^2}, \tag{28}$$

$$\dot{r}^2 = \left(\mathcal{E} - \frac{qe^{-\gamma}Q}{mr}\right)^2 - f(r)\left(\sigma + \frac{\mathcal{L}^2}{r^2}\right). \tag{29}$$

For timelike particles, one sets $\sigma = 1$. Introducing the specific energy $\mathcal{E} = E/m$ and setting $m = 1$ for simplicity (as is common in such analyses), the radial equation becomes:

$$\dot{r}^2 = \left(\mathcal{E} - \frac{qe^{-\gamma}Q}{r}\right)^2 - f(r)\left(1 + \frac{\mathcal{L}^2}{r^2}\right) \equiv \mathcal{E}^2 - V_{\text{eff}}(r;\mathcal{L},q). \tag{30}$$

and here, the effective potential V_{eff} is

$$V_{\text{eff}}^{\pm} = qA_t \pm \sqrt{f(r)\left(1 + \frac{\mathcal{L}^2}{r^2}\right)}. \tag{31}$$

The effective potential $V_{\text{eff}}(r;\mathcal{L},q)$ governs radial motion and includes contributions from both the ModMax charge term and the PFDM logarithmic correction.

Figure 3 shows the radial dependence of the effective potential for various parameters of charged ModMax BHs in PFDM. The top-left panel illustrates the effect of the ModMax parameter γ: as γ increases, the peak height decreases and its position shifts to larger radii, indicating a weakening of the potential barrier and a reduction in the effective gravitational attraction near the horizon. The top-right panel shows the dependence on the PFDM parameter α; increasing α yields a higher potential peak and shifts it toward smaller values of r/M, reflecting a stronger gravitational pull from the DM component. The bottom-left panel shows the effect of the BH charge Q: larger Q values produce a higher, broader potential barrier due to electrostatic repulsion, which partially offsets the gravitational contribution. Finally, the bottom-right panel displays the influence of the test particle's charge q: for negative q (opposite in sign to Q), the potential barrier increases due to electrostatic attraction, whereas for positive q it decreases. Collectively, these trends indicate that γ, α, Q, and q exert competing influences on the shape and height of the effective potential, thereby determining the character of stable and unstable orbits and the capture conditions for particles in DM-modified electrovacuum geometries.

A. Circular orbits of charged particles

The study of circular orbits of test charged particles around ModMax charged black holes in PFDM is carried out by imposing the conditions $V_{\text{eff}} = \mathcal{E}$ and $V'_{\text{eff}} = 0$, where the prime denotes differentiation with respect to r. Applying these conditions allows us to determine the angular momentum of a charged particle in circular motion.

From these conditions, we derive the expression for the angular momentum associated with circular orbits:

$$\mathcal{L}_\pm^2 = \frac{r^3}{(-2f + rf')^2}\left\{2f\left(q^2r(A_t')^2 + f'\right) - r(f')^2 \pm 2qfA_t'\sqrt{(qrA_t')^2 - 2(rf' - 2f)}\right\}. \tag{32}$$

The $\pm$ sign in Eq. (32) reflects symmetry with respect to the sign of the charge-coupling parameter qQ. The specific angular momentum is real only if the quantity under the square root is positive. This condition therefore implies:

$$(qr^2A_t')^2 \geq 2(rf'(r) - 2f(r)). \tag{33}$$

Figure 4 displays the dependence of the energy $\mathcal{E}$ of charged particles on the radial coordinate for circular orbits around charged ModMax BHs embedded in a PFDM

CPC Accepted

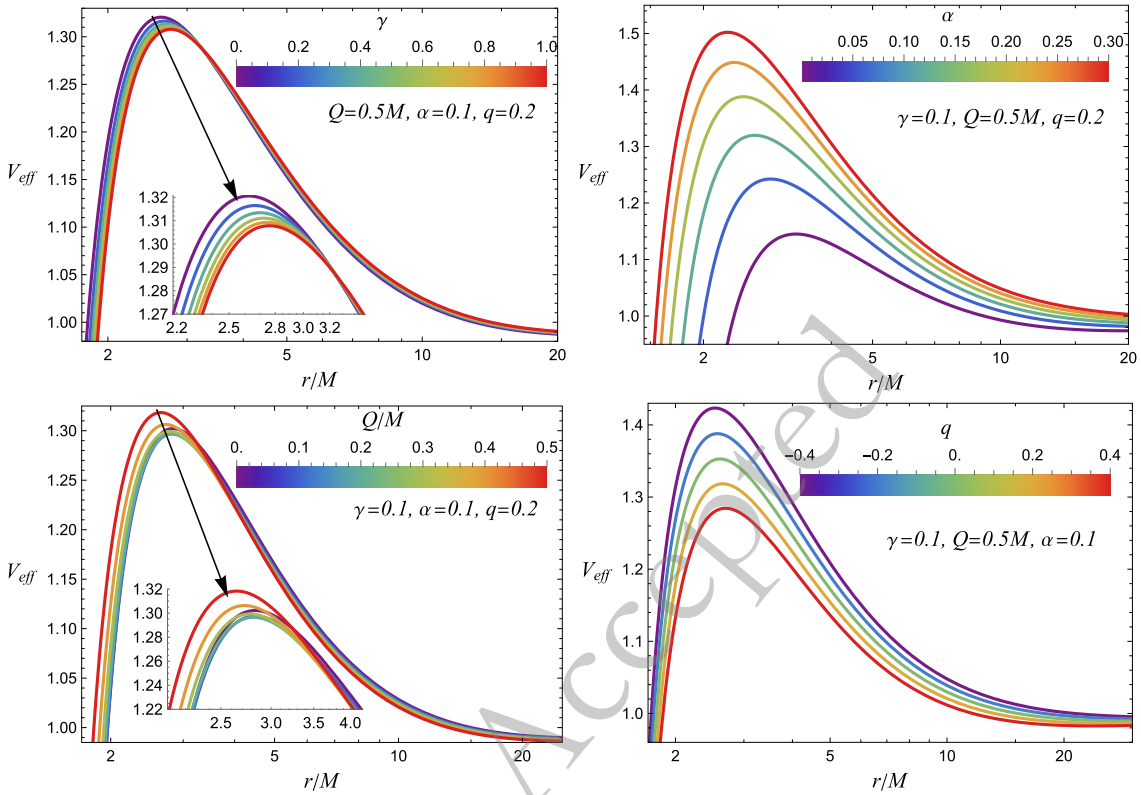

Fig. 3. (color online) Radial dependence of the effective potential for charged ModMax black holes in PFDM for various parameter values.

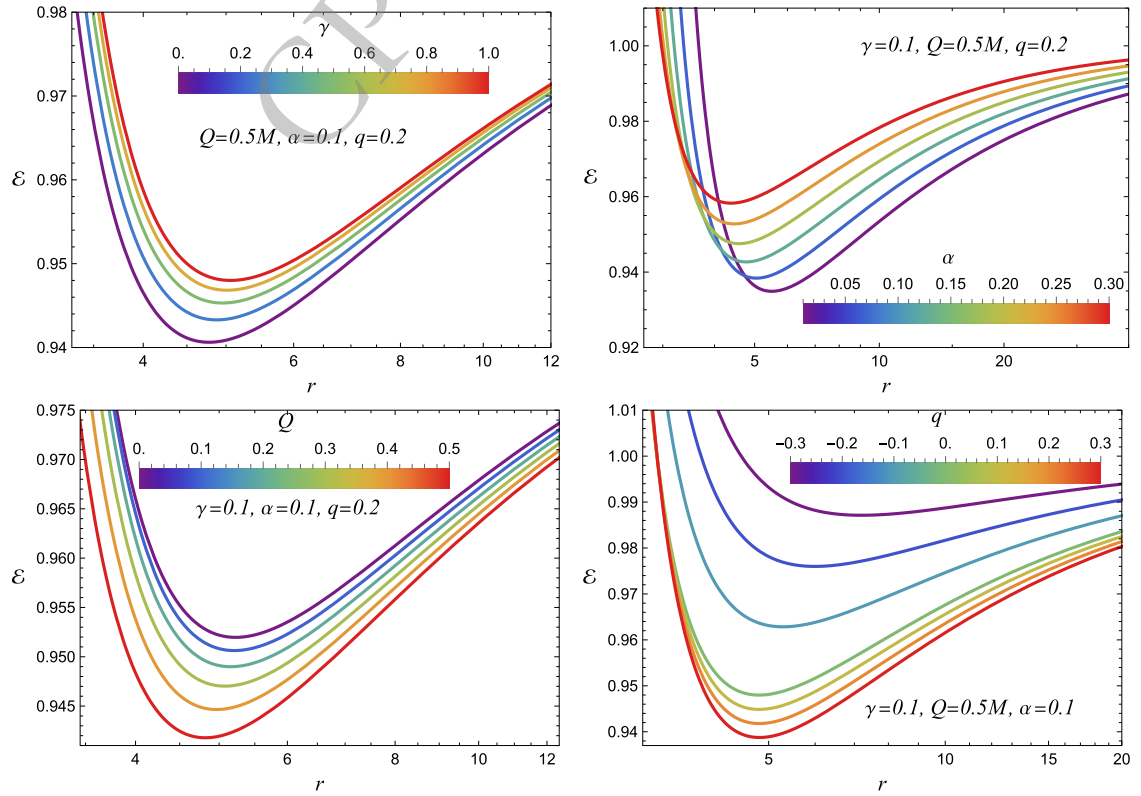

Fig. 4. (color online) Radial dependence of the energy $\mathcal{E}$ of charged particles in circular orbits around charged ModMax black holes surrounded by PFDM.

CPC Accepted

environment, for different model parameters. The top-left panel shows the effect of the ModMax parameter γ: as γ increases, the energy curves shift upward and their minima become shallower, indicating a weakening of the binding potential and a decrease in orbital stability. The top-right panel illustrates the effect of the PFDM parameter α; increasing α produces similar behavior—higher values of $\mathcal{E}$ and a smoother minimum —reflecting the DM-screening effect that weakens gravitational attraction. In contrast, the bottom-left and bottom-right panels, corresponding to the parameters Q and q, exhibit the opposite trend. Increasing the BH charge Q lowers the orbital energy $\mathcal{E}$ due to the strengthening of the electromagnetic interaction, thereby deepening the potential well; likewise, increasing the test-particle charge q (for charges of the same sign as Q) also leads to a reduction in $\mathcal{E}$ owing to electrostatic repulsion that counteracts gravitational attraction. Taken together, these results reveal opposite influences of (γ,α) and (Q,q) on the energetics of circular orbits: the former tend to weaken the binding field, raise energy levels, and reduce orbital stability, whereas the latter enhance the electromagnetic contribution, deepen the potential, and promote more energetically bound and potentially more stable configurations.

Figure 5 shows the radial dependence of the specific angular momentum $\mathcal{L}$ of charged particles moving in circular orbits around charged ModMax BHs embedded in a PFDM environment, for various choices of model parameters. The top-left panel illustrates the effect of the ModMax parameter γ: as γ increases, the values of $\mathcal{L}$ decrease and the minimum becomes less pronounced, indicating a reduced contribution from nonlinear electrodynamics and a lower angular momentum required to maintain circular orbits. The top-right panel shows the influence of the PFDM parameter α. Increasing α likewise reduces $\mathcal{L}$ and shifts the minimum toward smaller radii r/M, reflecting the weakening of the effective gravitational attraction due to the presence of PFDM. The bottom-left panel displays the effect of the BH charge Q, for which the behavior of $\mathcal{L}(r)$ is slightly non-monotonic: at smaller Q the angular momentum increases, whereas at larger Q it decreases slightly, reflecting competition between gravitational and electromagnetic effects. Finally, the bottom-right panel illustrates the dependence on the test particle charge q; increasing q yields higher $\mathcal{L}$ values, as electrostatic repulsion requires a larger angular momentum to maintain stable orbits.

Taken together, these results show that the parameters (γ,α) tend to reduce $\mathcal{L}$ and weaken the effective binding. By contrast, the parameters (Q,q) have the opposite effect, enhancing electromagnetic interactions and increasing the angular momentum required for stable circular motion. This contrast highlights the competing roles of nonlinear ModMax electrodynamics and charge effects in shaping particle dynamics in the ModMax–PFDM spacetime.

CPC Accepted

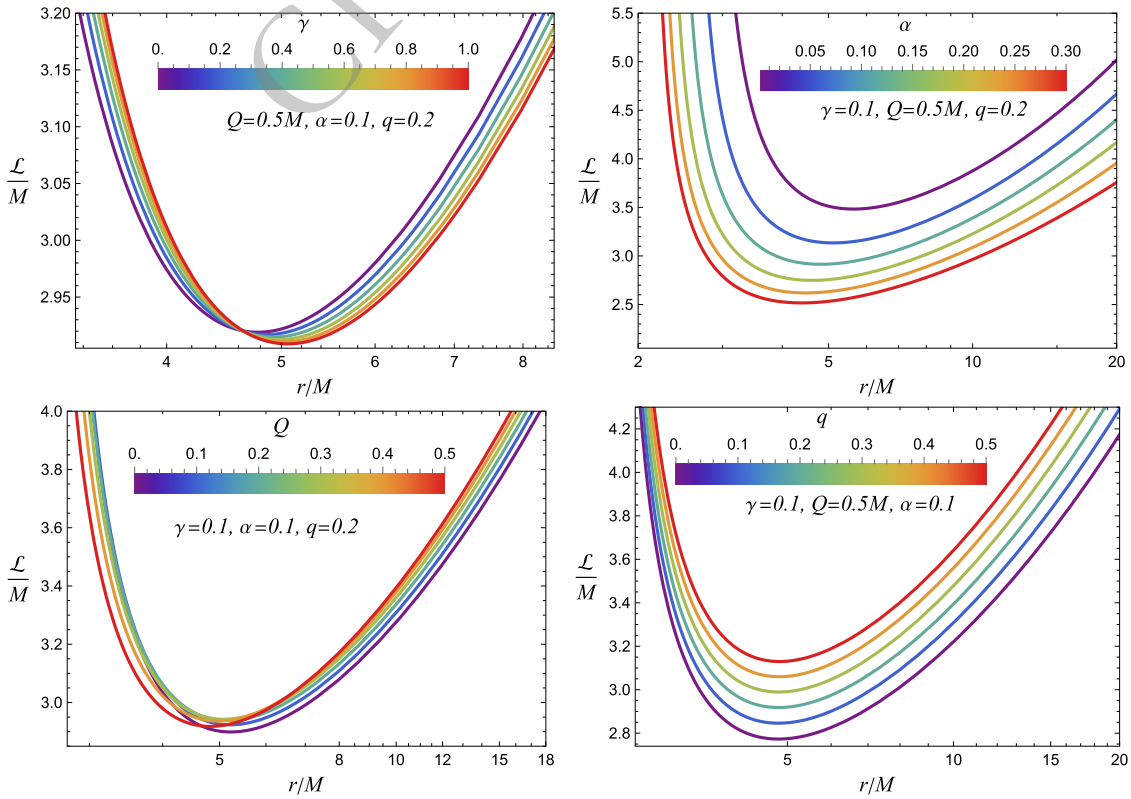

Fig. 5. (color online) Radial dependence of the angular momentum $\mathcal{L}$ for charged particles orbiting ModMax BHs in PFDM.

Figure 6 shows the relationship between the energy $\mathcal{E}$ and the angular momentum $\mathcal{L}$ for charged particles moving in circular orbits around charged ModMax BHs surrounded by PFDM. The top-left panel shows the influence of the ModMax parameter γ: as γ increases, the values of $\mathcal{L}$ decrease for a fixed $\mathcal{E}$, indicating a weaker electromagnetic contribution and a reduction in the angular momentum required to maintain a circular orbit. The top-right panel illustrates the effect of the PFDM parameter α: increasing α decreases $\mathcal{L}$, attributable to a weakening of the effective gravitational attraction induced by PFDM. The bottom-left panel illustrates the dependence on the BH charge Q: as Q increases, the required angular momentum $\mathcal{L}$ grows for a given energy, since electrostatic repulsion partially counteracts gravitational attraction. Finally, the bottom-right panel shows the influence of the test-particle charge q: when q increases (for charges of the same sign as Q), the required angular momentum rises due to electrostatic repulsion, whereas for opposite charge signs $\mathcal{L}$ decreases due to electrostatic attraction.

B. Innermost Stable Circular Orbit of charged particles

In this section, we study the ISCO of a charged particle around selected charged BHs [41, 42]. The stability of circular orbits is governed by the following conditions:

$$V_{\rm eff} = \mathcal{E}, \quad \partial_r V_{\rm eff} = 0, \quad \partial_{rr} V_{\rm eff} = 0, \tag{34}$$

Here, ∂_{rr} denotes the second-order derivative with respect to r. The vanishing of the first-order derivative characterizes stationary points, and the last condition corresponds to a minimum of the potential.

Figure 7 shows the dependence of the ISCO radius r_{ISCO} on the BH electric charge Q/M for different values of the ModMax parameter γ, the PFDM parameter α, and for particles with charges q of opposite sign.

The top-left panel illustrates the effect of γ for a positively charged particle ($q = 0.2$). The ISCO radius is asymmetric in Q: for negative Q, the orbits lie closer to the horizon, whereas for positive Q they move outward. Increasing γ has opposite effects in these two regimes: it increases r_{ISCO} for $Q < 0$ but decreases it for $Q > 0$. Thus, γ influences the orbital structure asymmetrically, enhancing or suppressing the effective Coulomb interaction depending on the relative signs of the charges.

The top-right panel shows the same dependence for a negatively charged particle ($q = -0.2$). Here, the trends are reversed: r_{ISCO} decreases with increasing γ for $Q < 0$

CPC Accepted

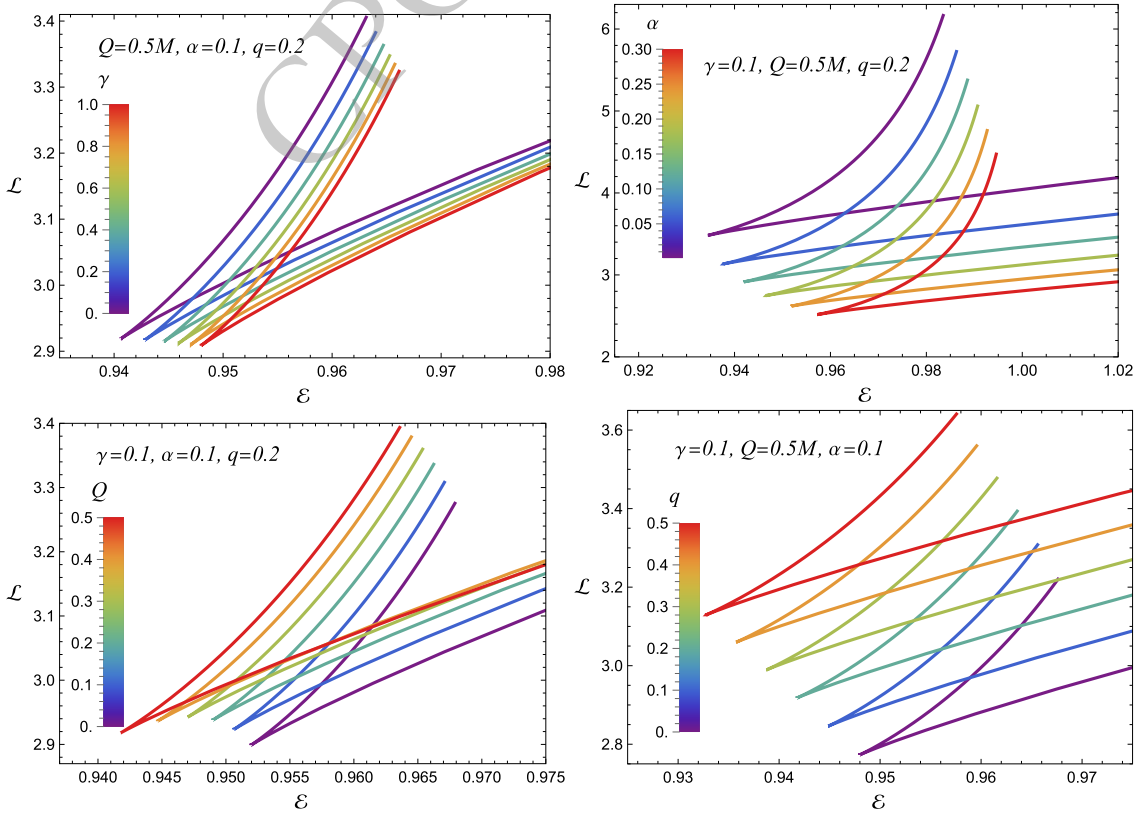

Fig. 6. (color online) The relationship between the energy $\mathcal{E}$ and the angular momentum $\mathcal{L}$ of charged particles on circular orbits around charged ModMax black holes in PFDM.

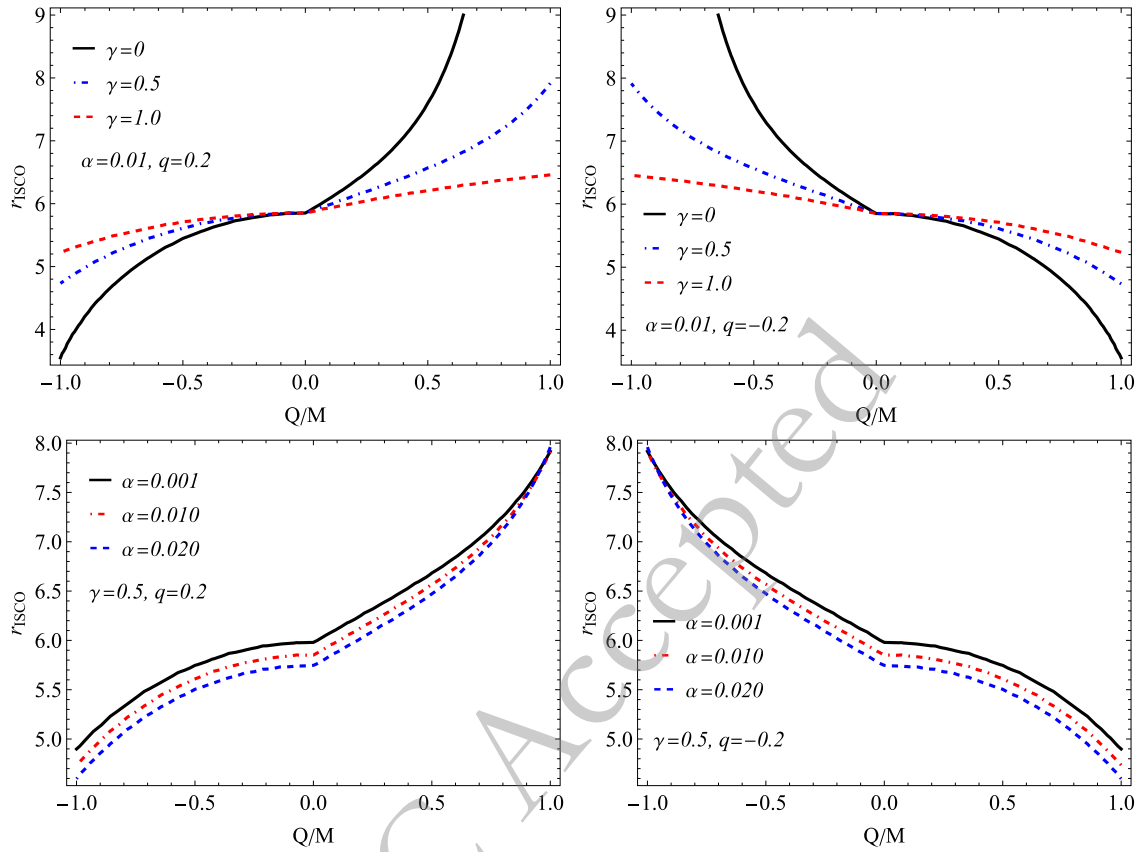

Fig. 7. (color online) Dependence of the ISCO radius on the BH charge in ModMax PFDM for positively and negatively charged test particles.

CPC Accepted

(like-charged configuration) and increases for $Q > 0$ (oppositely charged configuration). All curves intersect near $Q = 0$, where the effect of γ vanishes and r_{ISCO} coincides with the nearly-Schwarzschild value, slightly reduced by the PFDM contribution.

The bottom-left panel illustrates the effect of the PFDM parameter α for a positively charged particle. The ISCO radius grows with Q due to Coulomb repulsion, while increasing α reduces r_{ISCO}, indicating that the dark-matter component strengthens the effective binding. However, for $Q/M \approx 1$, all curves converge, implying that Coulomb interactions dominate and the PFDM effect becomes negligible.

The bottom-right panel shows the corresponding case for a negatively charged particle ($q = -0.2$). In this scenario, the trends are inverted: the ISCO radius decreases with increasing Q, since Coulomb attraction between opposite charges allows stable orbits closer to the horizon. As before, increasing α still reduces r_{ISCO}, but its influence weakens in the regime of strong Coulomb forces.

These results indicate that the parameters γ and α tend to stabilize the orbital configuration by reducing the ISCO radius. In contrast, the charge parameters Q and q introduce an asymmetry that determines whether the orbits shift inward or outward through the Coulomb interaction. The mirrored behavior upon reversing the sign of q highlights the internal consistency of the ModMax–PFDM framework.

IV. ELECTRIC PENROSE PROCESS

The electric Penrose process is a natural generalization of the classical Penrose mechanism, reformulated for BHs endowed with electric charge [30, 44]. In this scenario, energy extraction occurs when an incoming particle fragments in the near-horizon region of a charged BH. The particle splits into two fragments: one is absorbed by the BH, while the other escapes to infinity with energy exceeding that of the initial particle. The BH's electric charge is not merely incidental; it fundamentally alters the motion of charged particles, thereby increasing the efficiency of the extraction mechanism. Notably, even a small BH charge can yield a significant enhancement relative to the neutral case.

The conventional Penrose process has been studied in detail in the context of Kerr BHs, where rotational energy can be extracted through particle interactions within the ergosphere. This phenomenon underlies the amplification of superradiant modes and, under certain boundary conditions, can lead to the so-called "BH bomb" – a run-

away instability associated with repeated energy extraction [45−51]. In parallel, considerable effort has been devoted to analyzing how electric charge influences the effective potential landscape and the ISCO of charged particles. Remarkably, even a weakly charged BH can reproduce dynamical effects traditionally attributed to rotation, thereby extending the analogy between charged and rotating spacetimes [52].

These developments have profound implications for BH thermodynamics, the mechanisms underlying the formation of astrophysical jets, and a broader understanding of energy transport processes in highly curved spacetime. Building on these insights, numerous extensions of the Penrose process have been formulated for various BH configurations, encompassing both magnetic and electric variants [53, 54]. The present discussion focuses on the electric Penrose process in the context of charged ModMax BHs immersed in PFDM, highlighting the complex interplay among nonlinear electrodynamics, dark-sector effects, and high-energy particle dynamics.

A. Angular velocity, Conservation laws and maximum energy of ionized particle

Within the ModMax–PFDM spacetime described above, consider a charged particle approaching the BH from spatial infinity and decaying into two charged fragments in the equatorial plane near the event horizon. The decay satisfies the conservation of energy, angular momentum, electric charge, and radial momentum, expressed as:

$$E_1 = E_2 + E_3, \quad L_1 = L_2 + L_3, \quad q_1 = q_2 + q_3, \tag{35}$$

$$m_1\dot{r}_1 = m_2\dot{r}_2 + m_3\dot{r}_3, \quad m_1 \geq m_2 + m_3, \tag{36}$$

Here, E_i, L_i, q_i, and m_i denote the energy, angular momentum, electric charge, and mass of the i-th particle, respectively. Conservation of the ϕ-component of momentum is given by:

$$m_1 v_1^{\phi} = m_2 v_2^{\phi} + m_3 v_3^{\phi}, \tag{37}$$

Here, $v_i^{\phi} = \Omega_i v_i^t = \Omega_i e_i / r^2$, where $e_i = (E_i + q_i A_t)/m_i$ denotes the specific energy, and A_t is the time component of the electromagnetic four-potential.

To maximize the energy of the escaping fragment (particle 3), we assume that the initial particle is neutral ($q_1 = 0$) and at rest at infinity ($E_1 = m_1$, with specific energy $\mathcal{E} = 1$). The energy of particle 3 is then given by [31]:

$$E_3 = \frac{\Omega_1 - \Omega_2}{\Omega_3 - \Omega_2}(E_1 + q_1 A_t) - q_3 A_t. \tag{38}$$

Under the conditions $q_2 = -q_3$ and $q_1 = 0$, this simplifies to:

$$E_3 = \left(\frac{1}{2} + \frac{\sqrt{1 - f(r_i)}}{2}\right) E_1 - q_3 A_t, \tag{39}$$

where r_i denotes the radial coordinate at which the ionized particle is produced. In normalized form, the energy ratio is given by:

$$\frac{E_3}{E_1} = \left(\frac{1}{2} + \frac{\sqrt{1 - f(r_i)}}{2}\right) - \frac{q_3 A_t}{E_1}. \tag{40}$$

Maximum energy extraction occurs when q_3 and the BH charge Q have the same sign, owing to Coulomb repulsion, since A_t depends on Q.

Expressing the energy ratio explicitly, with $q_3 = Ze$ and $m_1 \approx Am_n$, where Z is the atomic number, e is the elementary charge, A is the mass number, and m_n is the nucleon mass, we obtain:

$$\frac{E_3}{E_1} = \left(\frac{1}{2} + \frac{\sqrt{1 - f(r_i)}}{2}\right) - \frac{ZeA_t}{Am_n c^2}. \tag{41}$$

The metric coefficient $f(r)$ and the component A_t depend on ModMax in the PFDM geometry, often leading to complex expressions that require numerical evaluation for accurate results [52].

The kinematics of the decaying particle are described by its four-velocity $v^{\alpha} = v^t(1, \mu, 0, \Omega)$, where $\mu = dr/dt$ is the radial velocity and $\Omega = d\phi/dt$ is the angular velocity. The normalization condition $v^{\alpha} v_{\alpha} = -\lambda$ (with $\lambda = 0$ for massless and $\lambda = 1$ for massive particles) yields:

$$(v^t)^2 \left[\frac{\mu^2}{f(r)} - f(r) + \Omega^2 r^2\right] = -\lambda. \tag{42}$$

The angular velocity as observed by a static observer at infinity is:

$$\Omega = \pm \frac{1}{v^t r} \sqrt{(v^t)^2 \left[f(r) - \frac{\mu^2}{f(r)}\right] - \lambda}, \tag{43}$$

constrained by:

$$\Omega_- \leq \Omega \leq \Omega_+, \quad \Omega_{\pm} = \pm \sqrt{\frac{f(r)}{r^2}}, \tag{44}$$

reflecting Keplerian orbits. For the decay scenario, the angular velocities are as follows [52]:

CPC Accepted

$$\Omega_1^2 = \frac{f(r)(1-f(r))}{r^2}, \quad \Omega_2 = \Omega_-, \quad \Omega_3 = \Omega_+. \tag{45}$$

Optimizing the energy gain by adjusting the angular momenta yields:

$$\frac{\Omega_1 - \Omega_2}{\Omega_3 - \Omega_2} = \frac{1}{2} + \frac{\sqrt{1-f(r_i)}}{2}. \tag{46}$$

This analysis assumes the ModMax solution in PFDM, which accounts for the BH's mass, charge, and angular momentum. The function $f(r)$ is typically the lapse function for ModMax in PFDM, given by Eq. 19, where α is the PFDM parameter. The process described resembles the Penrose process or its electromagnetic analog, in which energy is extracted via the BH's ergosphere or electromagnetic interactions. The energy ratio E_3/E_1 quantifies the efficiency of this mechanism and is critical for understanding high-energy astrophysical phenomena near BHs.

Figure 8 presents a comprehensive analysis of the energy-extraction efficiency, quantified by the ratio E_3/E_1, around charged ModMax BHs in PFDM. It shows how the efficiency depends on the BH electric charge Q under variations of three key parameters: the ModMax parameter γ, the PFDM parameter α, and the ionization radius r/M. In all cases, E_3/E_1 increases markedly with increasing Q, indicating that a stronger Coulomb field substantially enhances the acceleration of the ionized particle.

For a black hole of mass M, the characteristic charge at which the electric interaction becomes comparable to gravitational binding is $Q \sim \sqrt{G}M$, corresponding to $Q \sim 10^{20}$ C for a $10\,M_\odot$ black hole. Thus, even modest dimensionless values of Q/M represent extremely large charges in electromagnetic units, and in realistic astrophysical settings such charges are expected to be tightly constrained by plasma neutralization and pair creation.

The top-left panel shows E_3/E_1 as a function of the BH electric charge for several values of the ModMax parameter γ. The solid black curve represents the RN BH, the reference case. As γ increases, the curves shift downward, indicating that a larger γ weakens the efficiency of particle energy extraction (acceleration). For the same Q, BHs with higher γ yield smaller E_3/E_1, showing that the electromagnetic nonlinearity suppresses the Coulomb-driven energy gain. The top-right panel displays the effect of the PFDM parameter α on the efficiency. For all values of α, the curves are nearly identical because α does not contribute to the Coulomb interaction (20), which provides the dominant contribution to the efficiency (41).

CPC Accepted

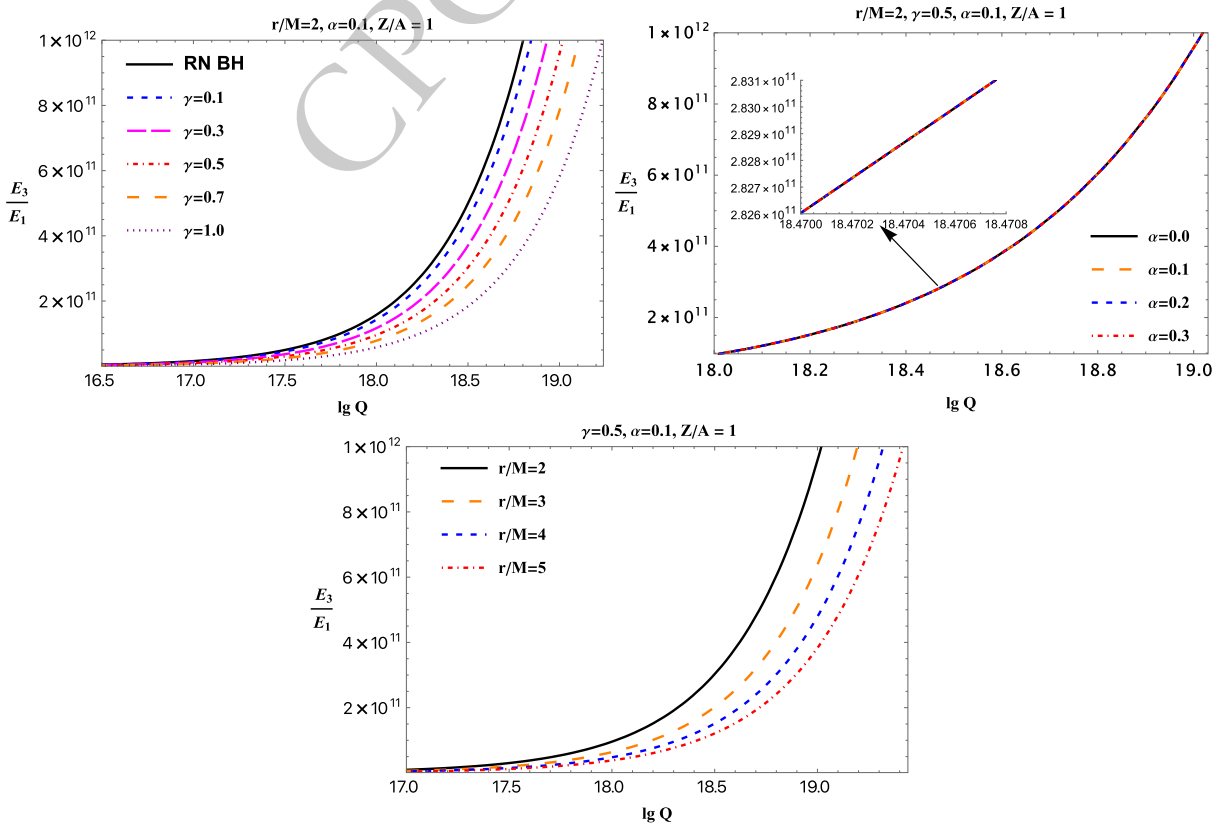

Fig. 8. (color online) The ratio of the extracted particle energies E_3/E_1 as a function of the black hole's electric charge $\lg Q$ for charged ModMax BHs immersed in PFDM with different parameter values.

The bottom panel shows the dependence on the ionization point: the farther the ionization occurs, the less efficient the electric Penrose process becomes, owing to the weakening of the Coulomb interaction.

Although the electric Penrose process considered here is formulated at the level of test-particle dynamics, it is instructive to place the extracted energies in a broader astrophysical context. In the stellar-mass and supermassive black hole cases, the characteristic energies released by the process are comparable, on a per-particle basis, to those associated with ultra-high-energy cosmic-ray protons and with relativistic jets in active galactic nuclei. However, the present analysis does not provide a realistic model of such complex astrophysical phenomena. Instead, the electric Penrose process serves as an idealized mechanism for quantifying the maximum energy extraction in near-horizon black-hole geometries and electromagnetic field configurations. In this sense, the results provide theoretical upper bounds on the energies of accelerated charged particles and qualitative insights into how ModMax electrodynamics and dark matter may influence energetic processes in strong-gravity regimes.

V. COLLISIONS OF CHARGED PARTICLES NEAR CHARGED MODMAX CHARGED BLACK HOLES IN PFDM

Bañados et al. [40] were the first to investigate the acceleration of particles colliding in the vicinity of spinning Kerr BHs, demonstrating that the center-of-mass energy of such collisions can, in principle, diverge in the case of an extremal Kerr BH. Following this seminal work, numerous studies have explored the influence of external magnetic fields on the acceleration mechanisms of charged particles near BHs within various gravitational frameworks and astrophysical scenarios [55−59].

In what follows, we define the critical angular momentum $\mathcal{L}_{cr}$ as the largest value of $\mathcal{L}$ for which a particle with fixed specific energy $E=1$, released from infinity, can still reach the horizon. Technically, $\mathcal{L}_{cr}$ is obtained by solving the simultaneous conditions $V_{\rm eff}(r;\mathcal{L}_{cr})=E$ and $\partial_r V_{\rm eff}(r;\mathcal{L}_{cr})=0$ at the corresponding turning point. For $\mathcal{L}>\mathcal{L}_{cr}$, the effective potential exhibits a forbidden region where $\dot{r}^2<0$, implying that such particles are reflected and cannot approach the near-horizon region, whereas for $\mathcal{L}\le\mathcal{L}_{cr}$ they can be captured and participate in near-horizon collisions.

The critical value of the angular momentum is obtained by imposing two conditions on the radial motion of the particle: (a) $\dot{r}=0$, which corresponds to a turning point of the trajectory, and (b) $d\dot{r}/dr=0$, which ensures an extremum of the radial-velocity function (see Figure 9). As the angular momentum increases ($\mathcal{L}>\mathcal{L}_{cr}$) beyond this threshold, the squared radial velocity becomes

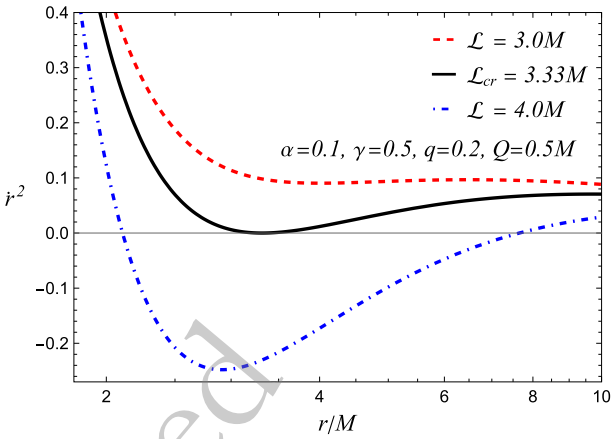

Fig. 9. (color online) Radial dependence of the square of the radial velocity of charged particles around a ModMax in PFDM for different angular momenta.

negative, indicating that particles are no longer able to approach the central object for such values. Accordingly, we examine the admissible range of angular momentum and determine the corresponding critical values.

Figure 9 shows the radial dependence of the squared radial velocity, $\dot{r}^2$, for charged particles orbiting a ModMax BH in PFDM for various angular momenta $\mathcal{L}$. Stable circular orbits exist only up to the critical value $\mathcal{L}_{cr}$, at which the effective potential admits such orbits. For smaller angular momentum (red dashed line), particles can approach the BH since $\dot{r}^2$ remains positive. However, for larger angular momentum (blue dot-dashed line), $\dot{r}^2$ becomes negative in some regions, indicating classically forbidden (imaginary) radial motion where physical trajectories cannot exist.

Figure 10 examines how $\mathcal{L}_{cr}$ varies with the PFDM parameter α (left panel) and the ModMax parameter γ (right panel) in the context of charged particle collisions near a ModMax BH in PFDM. The left panel shows that as the BH charge Q increases, the critical angular momentum $\mathcal{L}_{cr}$ either slightly increases or remains nearly constant, indicating that more highly charged BHs require a slightly larger critical angular momentum. As the PFDM parameter α increases, the curve shifts downward, i.e., $\mathcal{L}_{cr}$ decreases, implying that PFDM exerts a weakening influence. The right panel shows that the dependence of $\mathcal{L}_{cr}$ on BH charge Q is non-monotonic: as Q increases, the critical angular momentum first increases, reaches a maximum, and then decreases with further growth of Q. At $Q=0$, all curves coincide. Regarding the ModMax parameter γ, as γ increases, the curve shifts downward, implying that a larger γ reduces the critical angular momentum.

The center-of-mass energy for such collisions is given by [52, 58]:

CPC Accepted

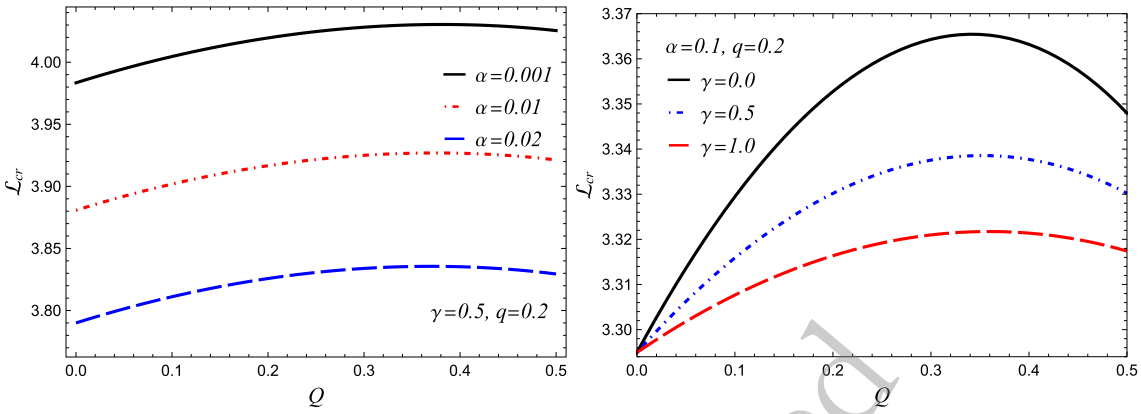

Fig. 10. (color online) Dependence of the critical angular momentum $\mathcal{L}_{cr}$ on α (left panel) and on γ (right panel) for various values of the black-hole and particle parameters.

$$\frac{E_{cm}^2}{m^2c^4} = A^2 + B^2 - 2g_{\mu\nu}u_1^\mu u_2^\nu, \tag{47}$$

where u_i^α denote the four-velocities of the particles, and for equal masses and energies ($E_1 = E_2 = m$):

$$\mathcal{E}_c^2 = \frac{E_c^2}{4m^2c^4} = 1 - g_{\alpha\beta}u_1^\alpha u_2^\beta\,. \tag{48}$$

In the equatorial plane ($\theta = \pi/2$), this reduces to:

$$\mathcal{E}_c^2 = 1 + \frac{1}{f(r)}(\mathcal{E}_1 - q_1A_t)(\mathcal{E}_2 - q_2A_t) + \frac{\mathcal{L}_1\mathcal{L}_2}{r^2} + \frac{1}{f(r)}\sqrt{(\mathcal{E}_1 - q_1A_t)^2 - f(r)\left(1 + \frac{\mathcal{L}_1^2}{r^2}\right)}\sqrt{(\mathcal{E}_2 - q_2A_t)^2 - f(r)\left(1 + \frac{\mathcal{L}_2^2}{r^2}\right)}\,. \tag{49}$$

The acceleration of charged particles near black holes, under the influence of external fields, has been investigated within various gravity models [56, 57]. Here, we examine head-on collisions between charged particles in the equatorial plane of a ModMax-KR black hole in a PFDM background. The center-of-mass energy is given by Eq. (49) [31, 52].

Figure 11 shows the radial dependence of the center-of-mass energy $\mathcal{E}_{\rm cm}$ for the collision of two charged particles near a charged ModMax BH in PFDM. The left panel illustrates the influence of the PFDM parameter α. One sees that the energy $\mathcal{E}_{cm}$ increases sharply as the particles approach the BH horizon, reaching a maximum at small radii, which reflects the characteristic Bañados–Silk–West (BSW) effect. An increase in the PFDM parameter α leads to a decrease in $\mathcal{E}_{cm}$ at all radii, since a higher DM density weakens the gravitational attraction and, consequently, reduces the kinetic energy of the particles at the collision.

The right panel demonstrates the effect of the nonlinear electrodynamics parameter γ. In contrast to α, an increase in γ causes the energy $\mathcal{E}_{cm}$ to grow, especially near the BH horizon. This occurs because stronger nonlinear electrodynamics increases the BH's effective charge, thereby strengthening the Coulomb repulsion between the

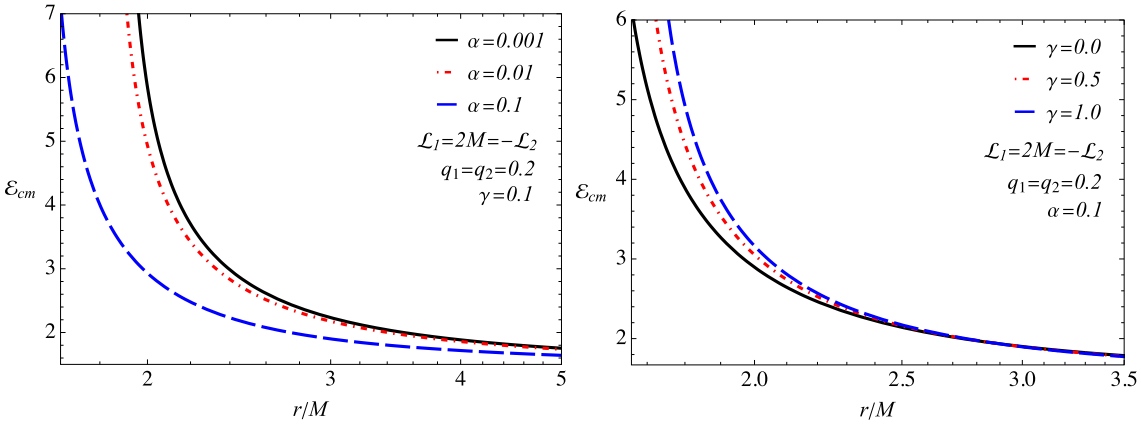

Fig. 11. (color online) Radial profiles of the center-of-mass energy $\mathcal{E}_{cm}$ near a charged ModMax black hole in PFDM, shown for different values of α (left panel) and γ (right panel).

CPC Accepted

charged particles and raising their relative velocity before the collision. Thus, the parameter γ enhances the BSW acceleration mechanism, whereas the parameter α suppresses it.

VI. CONCLUSION

This work has demonstrated that the parameters of ModMax nonlinear electrodynamics and the perfect-fluid dark matter (PFDM) component exert opposite effects on the orbital dynamics and energetic properties of charged particles in the vicinity of charged black holes. The ModMax nonlinearity parameter γ lowers the effective potential barrier and decreases the angular-momentum threshold for stable circular orbits, thereby weakening the electromagnetic interaction and leading to more extended orbital configurations. In contrast, increasing the PFDM parameter α enhances the effective gravitational attraction, raises the potential barrier, and shifts its minima toward smaller radii, resulting in more compact and tightly bound orbits.

For the ISCO radius, γ and α act in opposition. Increasing γ modifies r_{ISCO} asymmetrically with respect to the sign of the black hole charge: for negative Q, the ISCO radius increases, whereas for positive Q it decreases. The PFDM parameter α consistently reduces r_{ISCO}, although its effect becomes negligible at high charge values ($Q/M \approx 1$), where the Coulomb interaction dominates.

In the context of the electric Penrose process, the efficiency of energy extraction increases with the black hole charge due to stronger Coulomb repulsion between like-charged particles. However, increasing γ reduces this efficiency, while the influence of α remains weak and practically negligible. The energy gain also depends on the ionization radius, reaching a maximum when particle disintegration occurs near the event horizon.

The analysis of charged-particle collisions near the black hole horizon shows that the center-of-mass energy $\mathcal{E}_{cm}$ grows rapidly as the particles approach the horizon, exhibiting behavior characteristic of the Bañados–Silk–West (BSW) effect. The PFDM parameter α suppresses $\mathcal{E}_{cm}$ across all radii. In contrast, an increase in γ enhances it, particularly in the near-horizon region where the nonlinear electrodynamic effects of the ModMax theory become most significant.

From the detailed analytical and numerical results presented here, the distinct physical roles of PFDM in the ModMax black hole spacetime are clear. Unlike the ModMax parameter γ, the PFDM parameter α enters only through the spherically symmetric gravitational sector and does not contribute to the electromagnetic field potential. The parameter γ thereby enhances the effective charge of the black hole in a purely electric configuration. As a consequence, electromagnetic repulsion and charge–driven acceleration mechanisms become stronger, leading to higher escaping particle energies, extraction efficiencies, and center-of-mass energies near the horizon. In contrast, the PFDM parameter α modifies the spacetime geometry through an additional matter contribution to the energy–momentum tensor, producing an additional gravitational potential. This, in turn, enhances gravitational acceleration while reducing the kinetic energy available for extraction or high-energy collisions.

CPC Accepted

References

[1] D. Flores-Alfonso, B. A. González-Morales, R. Linares, and M. Maceda, Phys. Lett. B **812**, 136011 (2021), arXiv: 2011.10836[gr-qc]

[2] I. Bandos, K. Lechner, D. Sorokin, and P. K. Townsend, Phys. Rev. D **102**, 121703 (2020), arXiv: 2007.09092[hepth]

[3] Y. Sekhmani, S. K. Maurya, J. Rayimbaev, M. Altanji, I. Ibragimov, and S. Muminov, Physics of the Dark Universe **50**, 102116 (2025)

[4] A. Al-Badawi, F. Ahmed, and İ. Sakallı, Physics of the Dark Universe **50**, 102076 (2025), arXiv: 2508.03226[grqc]

[5] R. C. Pantig, L. Mastrototaro, G. Lambiase, and A. Övgün, European Physical Journal C **82**, 1155 (2022), arXiv: 2208.06664[gr-qc]

[6] K. Karshiboev, F. Atamurotov, A. Abdujabbarov, A. Övgün, and A. Reyimberganov, Communications in Theoretical Physics **76**, 025401 (2024)

[7] L. Meliyeva, O. Xoldorov, O. Tursunboyev, S. Karshiboev, S. Murodov, I. Nishonov, and B. Rahmatov, Chinese Physics C **49**, 125102 (2025)

[8] Y. Sekhmani, S. K. Maurya, J. Rayimbaev, M. Altanji, I. Ibragimov, and S. Muminov, Physics of the Dark Universe **50**, 102079 (2025)

[9] A. Al-Badawi, Y. Sekhmani, and K. Boshkayev, Physics of the Dark Universe **48**, 101865 (2025)

[10] K. Jafarzade, Z. Bazyar, and M. Jamil, Physics Letters B **864**, 139390 (2025), arXiv: 2411.15757[gr-qc]

[11] E. Ayón-Beato, D. Flores-Alfonso, and M. Hassaine, Phys. Rev. D **110**, 064027 (2024), arXiv: 2404.08753[hepth]

[12] D. N. Baker and M. Bodeau, in *Space Weather Effects and Applications*, Vol. 5, edited by A. J. Coster, P. J. Erickson, L. J. Lanzerotti, Y. Zhang, and L. J. Paxton (2021) p. 3, arXiv: 2106.07547[hep-th].

[13] I. Bandos, K. Lechner, D. Sorokin, and P. K. Townsend, Journal of High Energy Physics **2021**, 22 (2021), arXiv: 2012.09286[hep-th]

[14] K. Lechner, P. Marchetti, A. Sainaghi, and D. Sorokin, Phys. Rev. D **106**, 016009 (2022), arXiv: 2206.04657[hepth]

[15] Z. Avetisyan, O. Evnin, and K. Mkrtchyan, Phys. Rev. Lett. **127**, 271601 (2021), arXiv: 2108.01103[hep-th]

[16] K. Karshiboev, F. Atamurotov, A. Övgün, A. Abdujabbarov, and E. Karimbaev, New Astronomy **109**, 102200 (2024)

[17] S. I. Kruglov, International Journal of Modern Physics D **31**, 2250025 (2022), arXiv: 2203.11697[physics.gen-ph]

[18] B. E. Panah, Progress of Theoretical and Experimental Physics **2024**, 023E01 (2024), arXiv: 2402.12492[gr-qc]

[19] A. Ballon Bordo, D. Kubiznak, and T. R. Perche, arXiv e-prints, arXiv: 2011.13398 (2020), arXiv: 2011.13398 [hep-th].

[20] D. Flores-Alfonso, R. Linares, and M. Maceda, arXiv e-prints, arXiv: 2012.03416 (2020), arXiv: 2012.03416[grqc].

[21] D. Kubiznak, T. Tahamtan, and O. Svitek, arXiv eprints, arXiv: 2203.01919 (2022), arXiv: 2203.01919[grqc].

[22] Z. Amirabi and S. Habib Mazharimousavi, Eur. Phys. J. C **81**, 207 (2021), arXiv: 2012.07443[gr-qc]

[23] D. Hochberg and J. Pérez-Mercader, Phys. Rev. D **55**, 4880 (1997), arXiv: gr-qc/9609043[gr-qc]

[24] Z.-M. Xu, B. Wu, and W.-L. Yang, Physics Letters B **821**, 136632 (2021), arXiv: 2009.00291[gr-qc]

[25] Z. Xu, J. Wang, and X. Hou, Class. Quant. Grav. **35**, 115003 (2018), arXiv: 1711.04538[gr-qc]

[26] V. V. Kiselev, arXiv e-prints (2003), 10.48550/arXiv.grqc/0303031, arXiv: gr-qc/0303031[gr-qc].

[27] M.-H. Li and K.-C. Yang, Phys. Rev. D **86**, 123015 (2012), arXiv: 1204.3178[astro-ph.CO]

[28] J. Rayimbaev, U. Eshimbetov, B. Majeed, A. Abdujabbarov, A. Abduvokhidov, B. Abdulazizov, and A. Xalmirzayev, Chinese Physics C **48**, 055104 (2024)

[29] Y. Myrzakulov, O. Donmez, M. Koussour, S. Muminov, I. Y. Davletov, and J. Rayimbaev, Physics of the Dark Universe **48**, 101829 (2025), arXiv: 2407.08837[astro-ph.CO]

[30] R. Penrose, Riv. Nuovo Cim. **1**, 252 (1969)

[31] Z. Stuchlík, M. Kološ, and A. Tursunov, Universe **7**, 416 (2021)

[32] M. Kaplan, N. Raza, I. Davletov, I. Ibragimov, and S. Muminov, Physics Letters A **564**, 131079 (2025)

[33] Z. Yousaf, M. Z. Bhatti, M. Rizwan, J. Rayimbaev, I. Ibragimov, and I. Davletov, Nuclear Physics B **1019**, 117128 (2025)

[34] R. D. Blandford and R. L. Znajek, Mon. Not. R. Astron. Soc. **179**, 433 (1977)

[35] J. P. Lasota, E. Gourgoulhon, M. Abramowicz, A. Tchekhovskoy, and R. Narayan, Phys. Rev. D **89**, 024041 (2014), arXiv: 1310.7499[gr-qc]

[36] R. D. Blandford and D. G. Payne, Mon. Not. R. Astron. Soc. **199**, 883 (1982)

[37] M. Takahashi, S. Nitta, Y. Tatematsu, and A. Tomimatsu, Astrophysical Journal **363**, 206 (1990)

[38] L. Comisso and F. A. Asenjo, Phys. Rev. D **103**, 023014 (2021), arXiv: 2012.00879[astro-ph.HE]

[39] B. Chen, Y. Hou, J. Li, and Y. Shen, Phys. Rev. D **110**, 063003 (2024), arXiv: 2405.11488[gr-qc]

[40] M. Banados, J. Silk, and S. M. West, Phys. Rev. Lett. **103**, 111102 (2009), arXiv: 0909.0169[hep-ph]

[41] J. Rayimbaev, N. Kurbonov, A. Abdujabbarov, and W.- B. Han, Int. J. Mod. Phys. D **31**, 2250032 (2022)

[42] A. Demyanova, O. Rakhimov, Y. Turaev, N. Kurbonov, and J. Rayimbaev, in *RAGtime 20-22: Workshops on Black Holes and Neutron Stars*, edited by Z. Stuchlík, G. Török, and V. Karas (2020) pp. 19–27, proceedings of RAGtime 20-22.

[43] V. V. Kiselev, Class. Quant. Grav. **20**, 1187 (2003), arXiv: gr-qc/0210040

[44] A. Tursunov, B. Juraev, Z. Stuchlík, and M. Kološ, Phys. Rev. D **104**, 084099 (2021), arXiv: 2109.10288[gr-qc]

[45] R. Brito, V. Cardoso, and P. Pani, *Superradiance: New Frontiers in Black Hole Physics*, Lecture Notes in Physics, Vol. 971 (Springer Nature Switzerland AG, Cham, 2020) eBook ISBN: 978-3-030-46622-0, Second Edition.

[46] C. R. Almeida, Eur. Phys. J. H **46**, 20 (2021)

[47] C. A. R. Herdeiro and E. Radu, Phys. Rev. Lett. **112**, 221101 (2014), arXiv: 1403.2757[gr-qc]

[48] J. D. Bekenstein, Phys. Rev. D **7**, 949 (1973)

[49] J. D. Bekenstein and M. Schiffer, Phys. Rev. D **58**, 064014 (1998), arXiv: gr-qc/9803033

[50] W. H. Press and S. A. Teukolsky, Nature **238**, 211 (1972)

[51] Y. B. Zeldovich, Soviet Journal of Experimental and Theoretical Physics Letters **14**, 180 (1971)

[52] N. Kurbonov, J. Rayimbaev, M. Alloqulov, M. Zahid, F. Abdulxamidov, A. Abdujabbarov, and M. Kurbanova, Eur. Phys. J. C **83**, 506 (2023)

[53] N. Dadhich, A. Tursunov, B. Ahmedov, and Z. Stuchlík, Mon. Not. R. Astron. Soc **478**, L89 (2018), arXiv: 1804.09679[astro-ph.HE]

[54] M. Alloqulov, B. Narzilloev, I. Hussain, A. Abdujabbarov, and B. Ahmedov, Chin. J. Phys. **85**, 302 (2023)

[55] M. Zahid, J. Rayimbaev, N. Kurbonov, S. Ahmedov, C. Shen, and A. Abdujabbarov, Eur. Phys. J. C **84**, 706 (2024)

[56] A. A. Abdujabbarov, A. A. Tursunov, B. J. Ahmedov, and A. Kuvatov, Astrophys. Space Sci. **343**, 173 (2013), arXiv: 1209.2680[gr-qc]

[57] N. Kurbonov, A. H. Bokhari, J. Rayimbaev, and B. Ahmedov, European Physical Journal C **85**, 494 (2025)

[58] M. Zahid, S. U. Khan, and J. Ren, Chinese Journal of Physics **72**, 575 (2021), arXiv: 2101.07673[gr-qc]

[59] J. M. Ladino, C. A. Benavides-Gallego, E. Larrañaga, J. Rayimbaev, and F. Abdulxamidov, European Physical Journal C **83**, 989 (2023), arXiv: 2305.15350[gr-qc]

CPC Accepted